communications earth & environment

A Nature Portfolio journal

Article

https://doi.org/10.1038/s43247-026-03852-x

Projected impacts of future offshore wind farms on coastal precipitation over the Northwest European shelf

Check for updates

Naveed Akhtar [1] ✉, Alberto Elizalde[1], Beate Geyer[1] & Corinna Schrum [1,2]

Offshore wind energy plays a central role in reaching the European Green Deal target of a climate-neutral Europe by 2050. In this study, we simulate offshore wind development for 2023, 2030, and beyond 2050 across the Northwest-European Shelf, using various turbine sizes over a 10-year period, an approach not previously undertaken. For the post-2050 scenario, we assess the maximum potential deployment within all currently identified development zones in North Sea countries. Results indicate that large-scale offshore wind farm expansion can reduce surface wind speeds by up to 2–3 m s^{-1}. Notably for post-2050 scenario, precipitation decreases by 10–12% in coastal regions of Germany, the Netherlands, and the United Kingdom, and by more than 15% in parts of Jutland, Denmark, particularly under south-westerly winds. Conversely, precipitation increases over the wind farm areas. These findings suggest that extensive offshore wind deployment may significantly alter regional climate patterns, highlighting the need for further multi-model investigations to reduce uncertainty.

To reduce carbon emissions and limit the global average temperature increases above preindustrial levels below 1.5 °C, the European Commission aims to increase green energy, with significant contributions expected from offshore wind energy. In recent years, Europe has made significant progress in the use of wind energy, reaching 238 GW of onshore capacity and 34 GW of offshore capacity, totaling 272 GW of installed wind power. Within the European Union (EU), the total installed capacity is 220 GW, with 201 GW onshore and 19 GW offshore. By 2030, the EU aims to install 425 GW of wind energy capacity, which requires an average of 33 GW of new installations annually[1]. To meet this goal, the EU plans to increase its offshore wind capacity to 60 GW by 2030 and to 300 GW by 2050[2]. Supporting these targets, the North Seas Energy Cooperation (NSEC) has committed to achieving at least 260 GW of offshore wind capacity by 2050, which represents over 85% of the EU's offshore wind capacity target[3]. The North Sea is a major hub for offshore wind energy due to its unique features, such as strong, steady wind regimes, and shallow waters, which allow for the deployment of bottom-fixed wind turbines and other technologies far from the shore[4]. This indicates that the deployment of offshore wind installations in the North Sea is expected to increase significantly in the future (Fig. 1).

Offshore wind farms (OWFs) experience stronger and more consistent winds at sea compared to onshore wind farms[5,6]. Wind speeds about 10 km offshore are roughly 25% higher than on land, allowing 2–3 times longer power generation[7,8]. OWFs are typically clustered to maximize wind resource use and minimize infrastructure and operating costs. However, this clustering can lead to reduced power generation for downwind farms due to wakes created by upwind wind farms. Wind turbines generate wake areas of decreased wind speed and increased turbulence by extracting kinetic energy from the wind to convert some of it into electrical energy, and a part of it is dissipated as turbulent kinetic energy (TKE)[9–12].

Wind farms in the North Sea can substantially modify sea surface heat and momentum fluxes. These alterations not only enhance cloud cover and precipitation over wind farm areas but also exert a significant influence on the North Sea ecosystem[9,13,14]. Wind farms not only obstruct airflow within the rotor-swept area but also influence the atmosphere vertically, extending downward to the surface and upward to altitudes of approximately 400–500 m above hub height[9,10,14]. Furthermore, large OWFs can modify local and regional downwind climate by reducing wind speeds, enhancing TKE, and altering cloud and precipitation formation[15]. Observational evidence indicates that wakes can extend up to 50–70 km under stable atmospheric conditions[16]. Additionally, these wakes can affect the entire structure of the planetary boundary layer and modify the near-surface local flow [17–19]. Studies based on image analysis have shown that fog formation and dispersion over OWFs are influenced by increased mixing downwind of the farms[20,21]. Furthermore, a decrease in net upward sensible heat flux due to enhanced vertical mixing has been reported downwind of OWFs under stably stratified atmospheric conditions[22].

[1]Institute of Coastal Systems - Analysis and Modeling, Helmholtz-Zentrum Hereon, Geesthacht, Germany. [2]Center for Earth System Research and Sustainability, Institute of Oceanography, University of Hamburg, Hamburg, Germany. ✉e-mail: naveed.akhtar@hereon.de

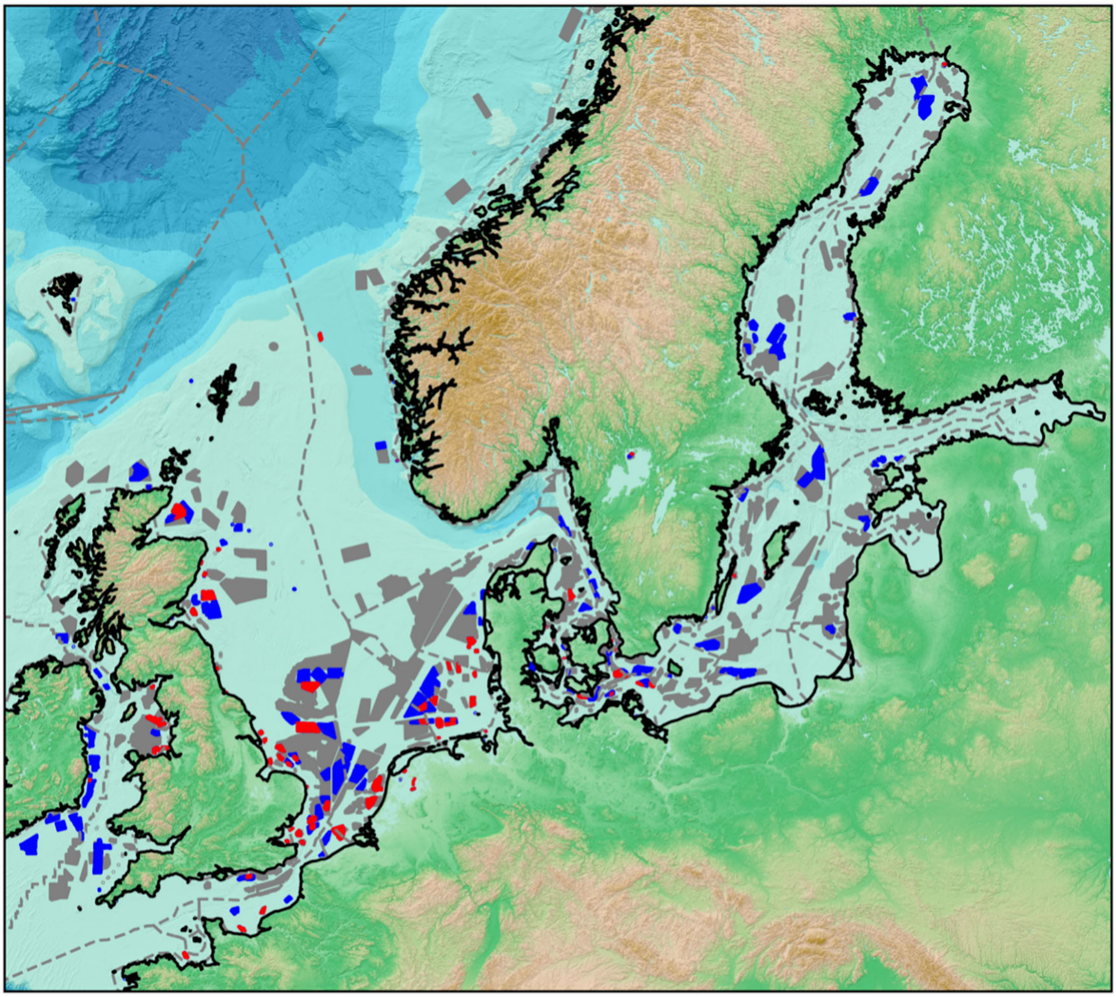

Fig. 1 | "Model domain and wind farm layouts". Planning status for OWFs (4c Offshore https://map.tgs4c.com/offshorewind, 2023) in the model domain used for technical scenario-setups for OWFs simulations: colored polygons indicate areas used in 2023 (red), in 2030 (blue), and 2050 (gray). The coastlines and orography are added for orientation purposes. This figure was created with Matplotlib (Hunter, J. D., Matplotlib: a 2D graphics environment. Computing in Science and Engineering 9, 2007) and Cartopy (Met office, Cartopy: a cartographic python library with a matplotlib interface. Exeter, Devon, https://scitools.org.uk/cartopy, 2015).

Recent in situ airborne measurements reveal that wakes can alter the local microclimate by changing temperature and humidity by approximately 0.5 K and 0.5 g/kg, respectively[23]. These changes at hub height are linked to variations in surface temperature and moisture, which, in turn, affect surface turbulent fluxes. Additionally, cloud formation above wind farms has been observed during airborne measurements under slightly stable conditions with nearly saturated relative humidity[20,24]. Numerical simulations, which represent wind turbines as momentum sinks and sources of TKE, suggest that OWFs have localized impacts on temperature, heat fluxes, clouds, and precipitation at both regional and global scales[9,25,26]. Additionally, these simulations have detected slight increases in temperature, clouds, and precipitation over OWFs[18,27,28]. Wind turbines enhance vertical mixing in the rotor area, leading to drying and heating near the surface, while moistening and cooling occur aloft. These energy budget alterations due to OWFs can subsequently influence the local climate[29].

Although OWFs are an important source of renewable energy and their deployment is expanding globally, the environmental impacts of these installations, particularly their influence on coastal precipitation, remain poorly understood[24]. A numerical study using a hypothetical OWF array found that during a hurricane, precipitation increases upstream and decreases by about 12% downstream of the wind farms[30]. This effect is attributed to wind speed reductions caused by turbines extracting kinetic energy, which induce convergence upstream and divergence downstream, altering local precipitation patterns. This hypothesis is supported by observations showing that nearshore OWFs can significantly reduce shoreline precipitation[31].

Previous studies provide evidence that OWFs can influence coastal precipitation patterns. However, further observational and numerical investigations are required to validate these findings. Considering the current limited number of OWFs compared to the ambitious deployment plans for 2050 and beyond, high-resolution climate models offer an opportunity to simulate the potential impacts of large-scale OWF scenarios such as those envisioned for the Northwest-European shelf on coastal precipitation. This raises a critical question: *What changes in coastal precipitation patterns can be expected as a result of local climate modifications induced by extensive OWF installations in Northwest Europe?*

To address this important question, we conducted simulations for the first time on the wind farms areas used in 2023, as well as the planning scenarios for 2030 and 2050 for OWFs in the Northwest-European shelf and Baltic Sea, as illustrated in Fig. 1. The data include both existing wind farms and installation plans projected through 2030 and 2050, which indicate a substantial expansion, particularly in the Northwest-European shelf. The impact of wind farms on regional climate also varies with turbine size[14]. We performed a simulation based on the 2023 installation areas with 5 MW turbines and another planning scenario for 2030 utilizing 10 MW turbine sizes. Additionally, we conducted three simulations for the 2050 planning scenario using 5 MW, 10 MW, and 15 MW turbines to investigate how turbine size influences the regional climate over a 10-year period (2008–2017). Although larger and more powerful turbines are expected to be deployed in the future, the 5 MW turbine is retained as a baseline to evaluate how scaling up to 10 MW and 15 MW influences local climate effects. Including this turbine ensures continuity with previous studies and allows for consistent comparison of results[9,14,27,28]. All experiments were conducted using the same capacity density of 8 MW/km². It should be noted that the simulations are based on a technical upper-limit offshore wind-farm scenario with a constant turbine density in all currently identified offshore wind developmental zones, while acknowledging that capacity density differs between countries and from wind farm to wind farm.

These simulations are exceptional due to the detailed wind farm planning data, extended integration time, and the large area they cover, which includes both the Northwest-European shelf and Baltic Sea. In this study, we focus on the impact of OWFs on coastal precipitation in this region.

Methods

COSMO-CLM model description and setup

In this study, we utilize the non-hydrostatic regional climate model COSMO-CLM 6.0[32] to simulate the effects of wind farms on local atmospheric dynamics for certain proposed wind farm scenarios in the Northwest-European shelf and Baltic Sea (as illustrated in Fig. 1). COSMO-CLM is a widely used regional climate model that has been extensively validated against observational datasets in numerous high-impact studies[27,32–34]. In addition to demonstrating the model's overall performance, earlier research[9,13,14,27,28,35] has specifically evaluated wind speed changes resulting from OWF parameterization, using both airborne measurements and mast data from FINO1[36]. More recently, another study[37] has provided further long-term validation of existing OWFs and placed particular emphasis on quantifying uncertainties.

The COSMO-CLM model uses the non-hydrostatic, compressible primitive equations on an Arakawa-C staggered grid. To better resolve the impact of wind farms we have used a uniform horizontal grid spacing of 0.045° (~5 km; 829 × 598 grid cells) and a vertically stretched grid with 62 terrain-following model levels. Our earlier studies[9,14,27] employed a ~ 2 km horizontal grid resolution over a smaller domain focused exclusively on the North Sea. In the present study, we adopt a substantially larger domain that includes the North Sea, the Baltic Sea, and the UK–Irish Sea region. To keep computational costs manageable for this expanded setup, we use a 5 km grid resolution. A comparison between the 5 km and 2 km configurations shows only minor differences, confirming that the coarser resolution is suitable for our purposes (see Supplementary Information (SI); Fig. SI 1). Similarly, an evaluation of different vertical resolutions indicates that a configuration with 61 levels provides the most appropriate and balanced performance for this study (for more details see SI, Fig. SI 2 and SI 3).

This configuration allows for 5 vertical levels within the rotor area of the 5 MW turbines, 7 vertical levels within the rotor area of the 10 MW turbines, and 8 vertical levels for the 15 MW turbines. The total heights of 5 MW, 10 MW, and 15 MW turbines are approximately 153 m, 218 m, and 270 m, respectively (see Table 1 for key parameters of the turbines used in this experiments). Time integration was carried out using a third-order Runge-Kutta scheme with a 30 s time step, while vertical turbulent diffusion was parameterized using a one-dimensional prognostic TKE advection scheme[38]. The model employs a delta-two-stream scheme to simulate longwave and shortwave radiation, incorporating a cloud microphysics scheme[38]. Initial and boundary conditions were derived from the coastDat3 simulations[33], which are available at hourly intervals on a 0.11° grid and utilized the European Centre for Medium-Range Weather Forecast (ECMWF) ERA-Interim reanalysis data as forcing. In addition to the atmospheric forcing, the model is constrained at the bottom boundary by prescribed sea surface temperatures, while surface roughness over the sea is calculated using the Charnock formula[39].

Table 1 | Key parameters of the wind turbines and wind farm used in the experiments

	5 MW	10 MW	15 MW
Hub height	90 m	119 m	150 m
Rotor diameter	126 m	198 m	240 m
Cut-in wind speed	3 ms^{-1}	3 ms^{-1}	3 ms^{-1}
Rated wind speed	11.4 ms^{-1}	11 ms^{-1}	10.5 ms^{-1}
Cut-out wind speed	25 ms^{-1}	25 ms^{-1}	25 ms^{-1}
Capacity density	8 MW/km²	8 MW/km²	8 MW/km²

Table 2 | Experiment names and their configurations

ID	Experiment name	Wind farms Status	Turbine size
1	NOWF	-	-
2	WF23_5MW	2023 operational and under construction	5 MW
3	WF30_10MW	2023 operational, under construction, and plans for 2030	10 MW
4	WF50_5MW	All plans for 2050	5 MW
5	WF50_10MW	All plans for 2050	10 MW
6	WF50_15MW	All plans for 2050	15 MW

Wind farm parameterization

A wind farm parameterization[25,35,40] has been integrated into the latest version 6 of COSMO-CLM to account for the effects of wind farms. This parameterization models the wind turbines as a sink of kinetic energy (KE) and a source of TKE in each layer intersecting the rotor area. The turbines convert a portion of the extracted KE into electrical power, while a part of it is transformed into TKE. The amount of KE extracted depends on factors such as wind speed, air density, turbine density, rotor diameter, and the thrust and power coefficients. The thrust and power coefficients, which vary with wind speed, are derived from the theoretical National Renewable Energy Laboratory (NREL) 5 and 10 MW, and International Energy Agency (IEA) 15 MW reference wind turbines for offshore system development[41,42]. The key parameters for the all three turbines used in this study, including values for cut-in, cut-out, and rated wind speeds, hub heights, rotor diameters, and capacity density are shown in Table 1.

Strategy for simulations and data analysis

We simulated atmospheric conditions for 10 years to capture a broad spectrum of weather patterns and assess the potential influence of large-scale OWF development on coastal precipitation. We selected the period 2008–2017 to be consistent with earlier studies where comparisons with different forcing data were made. These simulations incorporate all existing OWFs installation in the model domain for 2023 and technical future scenarios established for 2030 and 2050[43] (see Fig. 1). In total six simulations were performed using different wind turbine configurations. In this context, WFXX_YY refers to the COSMO-CLM simulations with wind farms, where "XX" denotes the existing wind farms for the year 2023 and future scenarios for the year 2030 and 2050, and "YY" indicates the turbine size of 5 MW, 10 MW, and 15 MW respectively. The simulations without wind farms are referred to as NOWF. Table 2 summarizes the key information about all the simulations and their experiment names.

The analysis focuses on annual and seasonal timescales over the period 2008–2017, using mean values from hourly datasets. The impact is assessed by comparing simulation results of operational wind farms as of 2023 and future scenarios of 2030 and 2050, utilizing turbines of various sizes, against control simulations without wind farms (see Tables 1 and 2). The direct

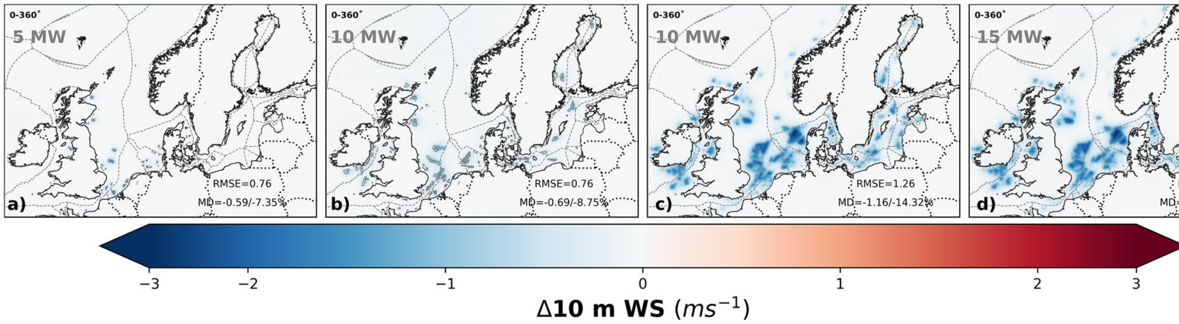

Fig. 2 | "Change in 10 m wind speed". Annual mean differences in 10 m wind speed between simulations with wind farms **a** WF2023_5MW, **b** WF2030_10MW, **c** WF2050_10MW, and **d** WF2050_15MW, and the control NOWF simulation for all wind directions (0—360°) over the period of 2008–2017. This figure was created with Matplotlib (Hunter, J. D., Matplotlib: a 2D graphics environment. Computing in Science and Engineering 9, 2007) and Cartopy (Met office, Cartopy: a cartographic python library with a matplotlib interface. Exeter, Devon, https://scitools.org.uk/cartopy, 2015).

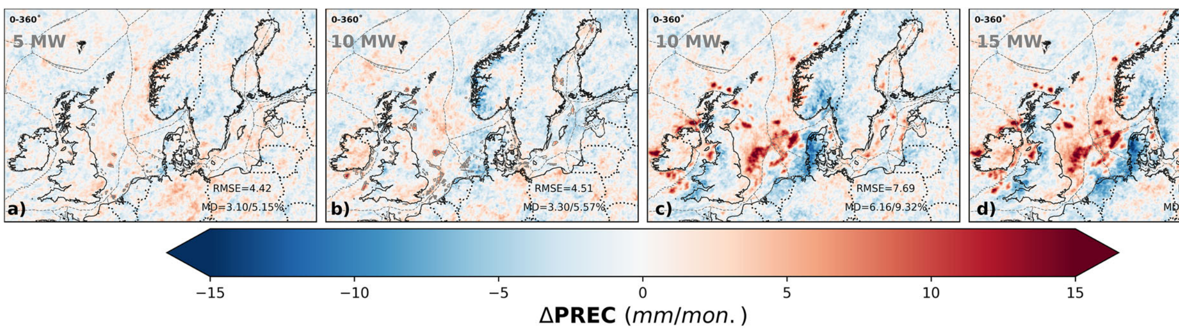

Fig. 3 | "Change in precipitation field". Annual mean differences in precipitation between simulations with wind farms **a** WF2023_5MW, **b** WF2030_10MW, **c** WF2050_10MW, and **d** WF2050_15MW, and the control NOWF simulation for all wind directions (0—360°) over the period of 2008–2017. This figure was created with Matplotlib (Hunter, J. D., Matplotlib: a 2D graphics environment. Computing in Science and Engineering 9, 2007) and Cartopy (Met office, Cartopy: a cartographic python library with a matplotlib interface. Exeter, Devon, https://scitools.org.uk/cartopy, 2015).

effects of the installed OWFs on wind speed were validated against mast and in-situ airborne measurements in a prior study[10].

Note that the total mean difference (MD) and root mean square error (RMSE) of annual and seasonal averages between the control and wind farm simulations, as shown in the figures, are calculated exclusively over the wind farm areas. Additional supporting analysis is provided in the SI.

Results and discussion

Impact of OWFs on surface wind speed

Our results indicate that as the number of OWFs increases, the reduction in 10 m wind speed becomes more pronounced, reaching values as strong as 2 to 3 ms^{-1} (Fig. 2 and Fig. SI 4). The magnitude of wind speed reduction over OWF areas is primarily influenced by turbine density, hub height, and rotor area. This localized decrease in wind speed subsequently affects air–sea fluxes, altering the exchange of momentum, heat, and moisture between the ocean surface and the atmosphere[14,31]. The impact of OWFs on surface fluxes can be reduced by replacing numerous smaller turbines with fewer, taller, and more powerful ones[31].

Impact of OWFs on precipitation

Our results demonstrate that existing wind farms under the 2023 and 2030 scenarios indicate small effects on precipitation, with effects primarily confined to marine areas. However, the large-scale deployment of OWFs in the Northwest-European shelf, as projected for 2050, has a significant and spatially distinct impact on regional precipitation patterns, specifically in the regions over northern Germany and Denmark, highlighting the critical role of scale and turbine density in driving these changes (Fig. 3 and Fig. SI 5). Simulations across all 2050 scenarios (5 MW, 10 MW, and 15 MW turbine capacities) consistently show a notable increase in precipitation ranging up to 8—10 mm/mon (12–18%) directly over the wind farm areas (see Fig. 3 for absolute difference and Fig. SI 6 for difference in percentage). In contrast, substantial reductions in precipitation, between 6 and 10 mm/mon (10–15%), are found in adjacent coastal regions of Denmark, Germany, the Netherlands, and western half of the United Kingdom (UK) when compared to control simulations without wind farms. The most pronounced decrease occurs in Jutland, Denmark, particularly around the area of Herning, which lies downwind of the Nordsøen I wind farm cluster located approximately 80 km off the Danish west coast (Fig. 4a). In Germany, the northwestern parts of Schleswig-Holstein and the coastal zones of Lower Saxony exhibit a reduction in precipitation of about 5–8 mm/mon (5–8%). Similarly, the Netherlands experiences a comparable 5–8% decrease in most of its areas, likely due to the proximity of many wind farm installations to the coastline. OWF installations in the Irish Sea lead to a reduction in precipitation along the west coast of the UK, estimated at approximately 5–8% (Fig. 4b). This reduction is likely driven by the prevailing south-westerly winds characteristic of Western Europe; consequently, similar decreases are not projected over Ireland or the eastern half of the UK, despite their proximity to future OWF sites. Additionally, the western half of the UK receives more precipitation due to orographic uplift, whereas the eastern half experiences less precipitation because of the rain-shadow effect.

These spatial patterns are robust across all three 2050 deployment scenarios, underscoring the consistent influence of large-scale OWF deployment on atmospheric moisture transport and precipitation distribution. Over the wind farm areas, the 2050 scenario simulations reveal a notable increase in precipitation. The largest increase occurs with 5 MW wind turbines, and 15 MW turbines (MD = 10.3%), followed by 10 MW turbines (MD = 9.3%). Importantly, the reduction in coastal precipitation is also more pronounced in 2050 scenarios with 5 MW turbines (Fig. SI 6).

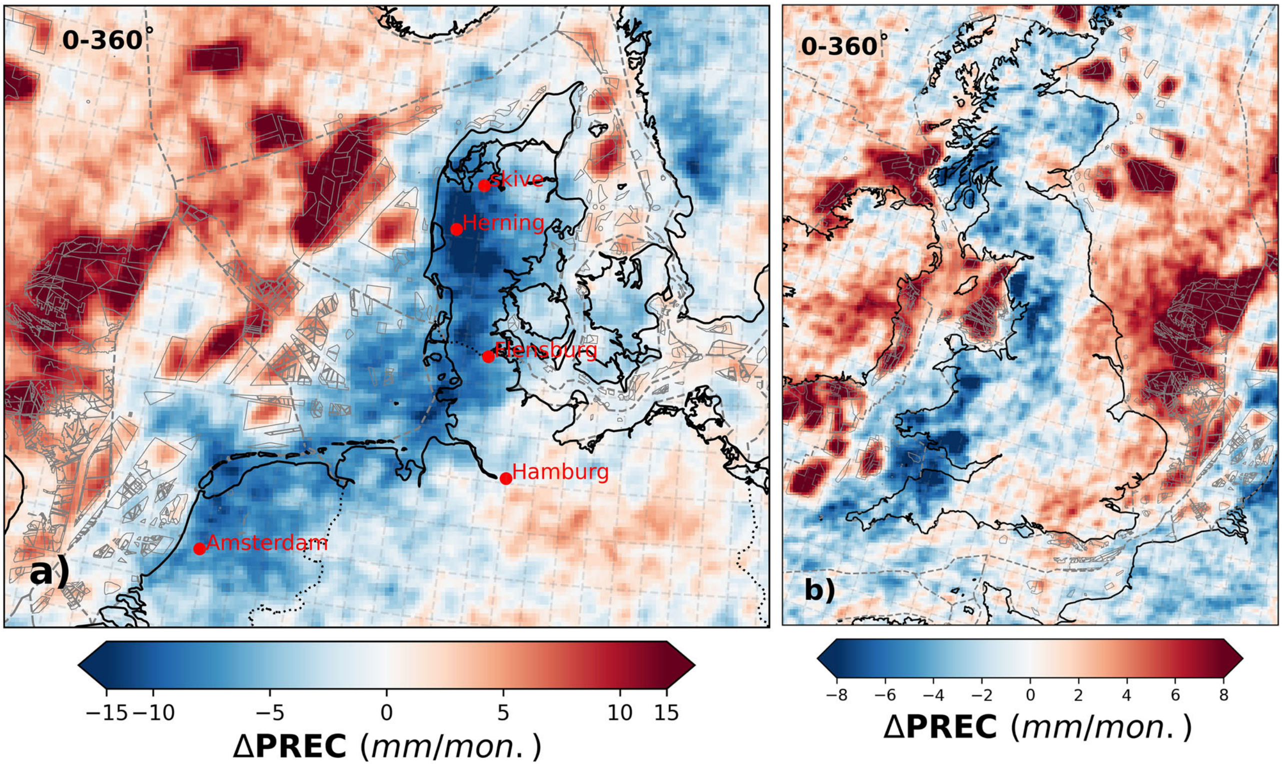

Fig. 4 | "Change in precipitation field". Annual mean differences in precipitation between simulations with wind farms WF2050_15MW and control NOWF simulation for all wind directions (0—360°) over the period of 2008–2017 **a** for Germany, Denmark and the Netherlands and **b** for UK. This figure was created with Matplotlib (Hunter, J. D., Matplotlib: a 2D graphics environment. Computing in Science and Engineering 9, 2007) and Cartopy (Met office, Cartopy: a cartographic python library with a matplotlib interface. Exeter, Devon, https://scitools.org.uk/cartopy, 2015).

Fig. 5 | "Change in vertical wind speed". Annual mean differences in vertical wind speed at 150 m height between simulations with wind farms WF2050_15MW and control simulation (NOWF) for wind directions from 200 to 280 °over the period of 2008–2017. This figure was created with Matplotlib (Hunter, J. D., Matplotlib: a 2D graphics environment. Computing in Science and Engineering 9, 2007) and Cartopy (Met office, Cartopy: a cartographic python library with a matplotlib interface. Exeter, Devon, https://scitools.org.uk/cartopy, 2015).

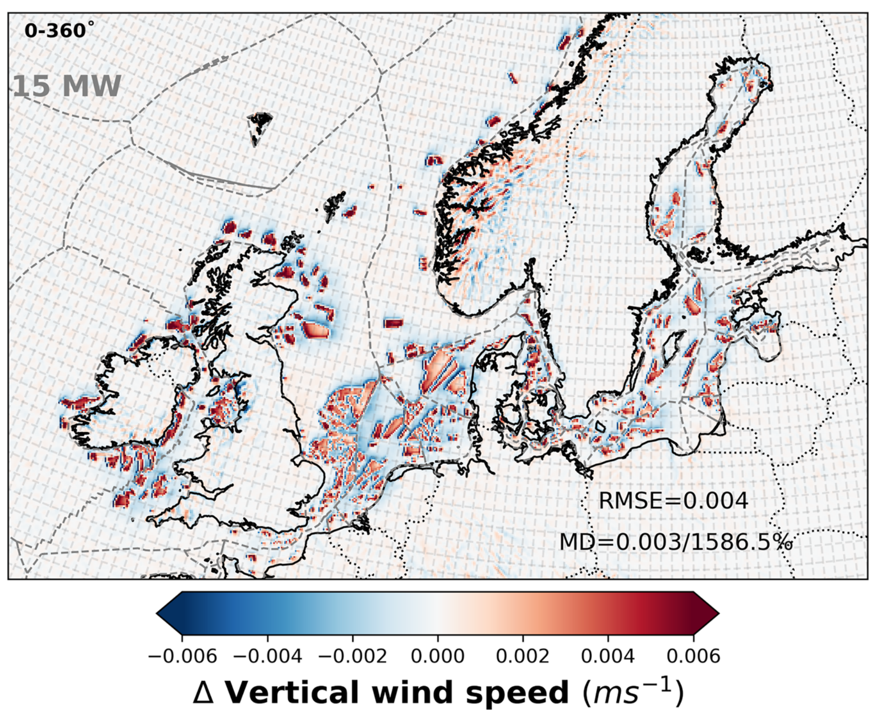

This is due to the higher turbine density of 5 MW units, which results in a greater overall increase in TKE and enhanced advection of moisture.

The statistical evaluation of precipitation differences shows spatially coherent regions of significant change, with |t| values exceeding 5 in several OWF areas. Corresponding p-value patterns ($p < 0.05$–0.10) confirm that these precipitation responses are locally significant. These results demonstrate that the modeled precipitation impact of OWFs is not random but represents a structured and detectable signal (see Fig. SI 7).

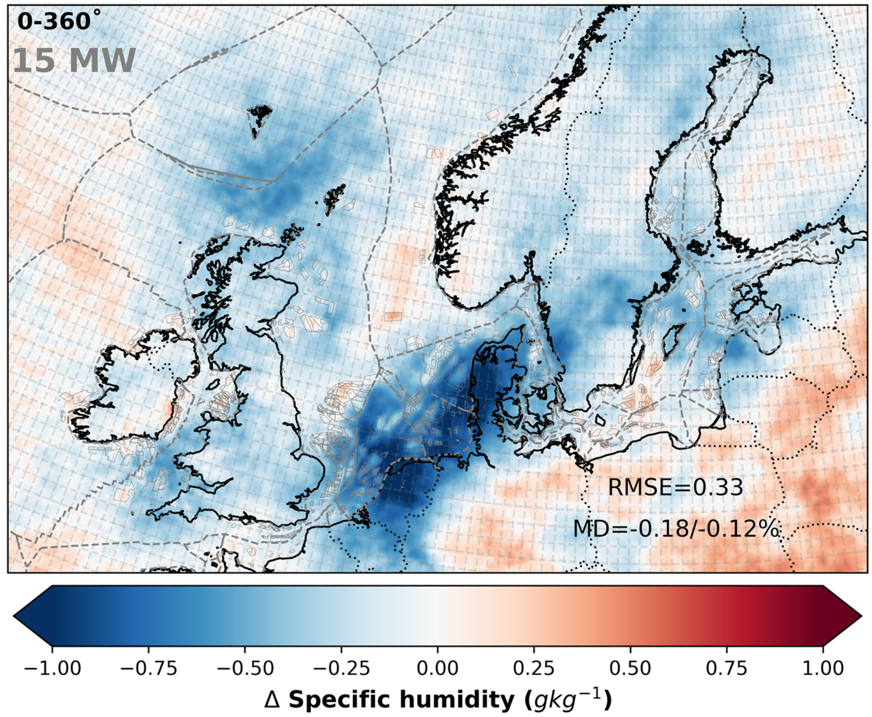

Fig. 6 | "Change in specific humidity". Annual mean differences in specific humidity between the simulation with wind farms WF2050_15MW and control simulation (NOWF) for wind directions from 200 to 280° over the period of 2008–2017. This figure was created with Matplotlib (Hunter, J. D., Matplotlib: a 2D graphics environment. Computing in Science and Engineering 9, 2007) and Cartopy (Met office, Cartopy: a cartographic python library with a matplotlib interface. Exeter, Devon, https://scitools.org.uk/cartopy, 2015).

A detailed analysis of daily precipitation data over central Jutland revealed that the number of precipitation days over land is projected to remain constant. Therefore, the reduction in total precipitation is attributed to a shift from high-intensity to lower-intensity events. In contrast, over the Nordsøen I wind farm area located upwind of Jutland the number of precipitation events is projected to increase slightly by 3%, with a corresponding shift toward higher-intensity events (see Fig. SI 8).

In the Northwest-European shelf, south-westerly winds are the dominant force[10,44] (Fig. SI 9). Our results reveal that the reduction in precipitation around the coastal regions of Denmark, Germany, and the Netherlands mainly occurs during dominant south-westerly wind conditions (Fig. SI 10). During these prevailing winds, precipitation over the wind farm increases up to 5—10 mm/mon (9—20%), while adjacent coastal regions experience a reduction of about 5–8%. Specifically, under the 2050 scenario, simulations indicate a mean increase in precipitation of approximately MD = 19% over the wind farm areas, highlighting the spatial redistribution of precipitation driven by large-scale offshore wind farm deployment. This indicates that the presence of wind farms can enhance local precipitation over the wind farm areas while simultaneously reducing it along the coast.

The influence of the OWFs on coastal precipitation varies considerably with wind direction (Fig. SI 11). The strong impact we found for the prevailing winds is not found for northwesterly winds (280° to 360°) which occur with high frequencies as well. They exhibit negligible impact on precipitation in the coastal regions (Fig. SI 11c). The same holds for the relatively rare winds originating from 0° to 100°, and 100° to 200°, showing minimal influence on coastal precipitation patterns (Fig. SI 11a and 11b). The reduction in coastal precipitation is primarily driven by south-westerly winds (200–280°) which dominate the Northwest-European shelf for most of the year and play a key role in moisture transport and precipitation dynamics. This influence is evident across all seasons except spring, when south-westerly winds are less prevalent in the region. During the winter and autumn seasons, precipitation decreases up to 8—15 mm/mon (10 to 20% Fig. SI 12 and SI 13; for more detail see SI).

Our results indicate that increases in precipitation over offshore wind farm areas are most pronounced when wind speeds range between 12 and 25 ms^{-1} corresponding to the operational range in which turbines typically rotate at or near their rated capacity. In contrast, the reduction in precipitation over adjacent land areas is more significant when wind speeds fall between 3 and 12 ms^{-1} (Fig. SI 14). These wind speed ranges are critical, as they determine the extent of turbine-induced atmospheric disturbances. Wind farms are considered inoperative at wind speeds below 3 ms^{-1} and above 25 ms^{-1}, resulting in negligible changes in wind speed and precipitation during these conditions. This highlights the importance of wind speed variability in modulating the spatial distribution of precipitation associated with large-scale wind farm deployment.

To examine how wind turbines affect vertical mixing and atmospheric water content, we analyze vertical wind speed, divergence patterns at hub height, and the total vertically integrated water content. Over the wind farms, the vertical wind speed difference is positive by approximately 0.003 ms^{-1} at a hub height of 150 m (Fig. 5), enhancing upward motion and moisture transport and though increasing low cloud cover and precipitation. Conversely, downstream of the wind farms, the vertical wind speed difference turns negative, suppressing upward motion and reducing cloud formation and precipitation. This is confirmed by the analysis of the horizontal wind divergence difference, which is negative over the wind farms because the wind slows down as it encounters the turbines. Downstream, the divergence difference becomes positive as the wind speed recovers past the wind farms (Fig. SI 15). The t-statistic map exhibits spatially coherent bands of positive and negative values aligned with OWF footprints and coastal features, with |t| frequently exceeding 5 and reaching ~20 in several corridors. The p-value map shows extensive areas with $p < 0.05$–0.10, indicating that differences between CCLM_WF and CCLM are locally significant across large portions of the OWF domains. The consistency between high |t| regions and low p-values confirm a structured, statistically detectable signal (see Fig. SI 16).

While the enhanced vertical mixing and divergence increases the cloud formation and favors precipitation, the specific humidity of the atmosphere is reduced downwind of the wind farm areas (Fig. 6). The enhanced precipitation over the wind farms reduces the moisture content in the atmosphere. The transport of the drier air includes even far areas and is reaching the coasts leading to reductions in precipitation there. At higher wind speeds, moisture exchange becomes more intense, which helps maintain atmospheric water content. As a result, the reduction in precipitation is less pronounced compared to situations with lower wind speeds. Our results are supported by previous findings on changes in coastal precipitation due to OWF installations, as identified by an earlier modeling study[30] and observational analyses[31].

Conclusions

This study investigates the regional-climate impacts of offshore wind farms by applying different technical scenarios for 2023, 2030 and 2050. The 2050 scenario is designed as an upper-bound estimate reflecting the maximum feasible level of installation within the designated development zones. Our findings based on the simulation using 2050 scenario indicate that a large-scale intense deployment of OWFs, could lead to a reduction in precipitation of approximately 8% to 15% in coastal regions of Denmark, Germany, the Netherlands, and the United Kingdom, particularly during the winter and autumn seasons. Regional climate projections under the RCP8.5 scenario, reported independently in the literature, indicate a general increase of around 15% in winter precipitation across much of Northern Europe, including Denmark and Germany[45]. Importantly, our OWF experiments do not aim to replicate or replace these scenario-based climate projections. Instead, they highlight the potential regional-scale meteorological effects associated with extensive OWF deployment. No consistent signal emerges for summer precipitation in our simulations. According to the IPCC AR6 Europe Fact Sheet, precipitation changes regardless of scenario are generally more pronounced in winter than in summer[46]. The results highlight an important limitation of IPCC AR6 GCM simulations, which do not explicitly represent the regional and local climatic effects of offshore wind farm (OWF) development. This helps explain discrepancies between large-scale projections and the findings of this study. In contrast, high-resolution regional climate models such as COSMO-CLM are better suited to capturing OWF-induced mesoscale processes, underscoring their value for robust climate assessments at smaller spatial scales in the context of sustainable energy transitions.

Our results also highlight the potential for OWFs to reduce moisture transport from sea to land, emphasizing the complex interplay between wind farm placement, prevailing wind directions, and precipitation patterns. The simulations are based on upper-limit OWF deployment plans, employing a capacity density of 8 MW/km^2, and are derived from a single atmospheric model, one wind-farm scenario, and a specific capacity configuration. Consequently, further research employing multiple atmospheric models, a broader range of wind-farm capacity densities, and varying spatial extents is required to better constrain uncertainties and to robustly assess the magnitude and realism of these impacts. Future studies should also move beyond mean climatological responses to examine hydroclimatic extremes such as storm surge, and flood risks which are critical for regional impact assessments and adaptation planning.

Given that precipitation responses are highly sensitive to model configuration including numerical schemes, turbulence parameterizations, and resolution sensitivity analyses are recommended to identify thresholds in OWF deployment that may trigger significant reductions in coastal precipitation. Additionally, it is important to evaluate the implications of these scenarios for marine ecosystems and physical ocean processes to ensure a comprehensive understanding of environmental impacts and support sustainable offshore development.

Data availability

The FINO1 wind speed observational data used in this study are publicly available and can be accessed free of charge through the FINO1 data repository: https://www.fino1.de/en/news-data/live-data.html. The offshore wind farm layout data used in this study were obtained from 4 C Offshore (https://map.tgs4c.com/offshorewind/) and are subject to licensing restrictions; therefore, these data are not publicly available but may be obtained directly from the data provider under the applicable license terms. The coastDat3 data used to provide boundary and forcing conditions for the climate model are also publicly available and can be accessed through the coastDat data archive (www.wdc-climate.de/ui/entry?acronym=coastDat-3_COSMO-CLM_ERAi). The COSMO-CLM_WF and COSMO-CLM model datasets supporting the findings of this study, as well as the COSMO-CLM namelists, are available from the authors upon request. The COSMO-CLM simulations were conducted using the community-wide, publicly accessible COSMO-CLM code (https://www.clm-community.eu). All the model datasets can be obtained from the corresponding author upon request. The key offshore wind turbine parameters used in this study were derived from the NREL offshore wind turbine reference models, which are publicly available (https://natlabrockies.github.io/turbine-models/index.html). All source data and the numerical results underlying the figures presented in the main article are available on Figshare (Project - Projected impacts of future offshore wind farms on coastal precipitation over the Northwest European shelf - Figshare).

Code availability

The COSMO-CLM (CCLM) model is developed and maintained by the Climate Limited-area Modeling Community (CLM-Community). The model source code is not publicly distributed without restriction but is available to members of the CLM-Community under a license agreement. Access to the COSMO-CLM code can be requested via the CLM-Community website (https://www.clm-community.eu). The code of wind farm parameterization implemented in the model is publicly available through Zenodo (https://doi.org/10.5281/zenodo.10069391). All figures in this study were generated using the Python libraries Matplotlib (Hunter, 2007) and Cartopy (Met Office, 2015). Matplotlib was used for plotting and visualization, and Cartopy was used for geospatial mapping and cartographic visualization.

Received: 8 August 2025; Accepted: 16 July 2026;
Published online: 12 August 2026

References

1. WindEurope. Wind Energy in Europe. In *Statistics and outlook* (WindEurope, 2024).
2. European Commission Directorate-General for Energy; DVN; Artelys; Trinomics; Andrey, C. et al. Offshore Renewable Energy and Grids – An Analysis of Visions towards 2050 for the Northern Seas Region and Recommendations for Upcoming Scenario-Building Exercises. *Publ. Off.* https://doi.org/10.2833/693330 (2022).
3. North Seas Energy Cooperation. Joint Statement on the North Seas Energy Cooperation-12 Sept 2022. **14**, 1–6 https://www.benelux.int/wp-content/uploads/2023/02/dublin-statement.pdf (2021).
4. Sherman, P., Chen, X. & McElroy, M. Offshore wind: an opportunity for cost-competitive decarbonization of China's energy economy. *Sci. Adv.* **6**, 1–9 (2020).
5. Zheng, C. W., Li, C. Y., Pan, J., Liu, M. Y. & Xia, L. L. An overview of Global Ocean wind energy resource evaluations. *Renew. Sustain. Energy Rev.* **53**, 1240–1251 (2016).
6. Kaplan, Y. A. Overview of wind energy in the world and assessment of current wind energy policies in Turkey. *Renew. Sustain. Energy Rev*. https://doi.org/10.1016/j.rser.2014.11.027 (2015).
7. Tambke, J., Lange, M., Focken, U., Wolff, J. O. & Bye, J. A. T. Forecasting offshore wind speeds above the North Sea. *Wind Energy* **8**, 3–16 (2005).
8. Wang, J., Qin, S., Jin, S. & Wu, J. Estimation methods review and analysis of offshore extreme wind speeds and wind energy resources. *Renew. Sustain. Energy Rev*. https://doi.org/10.1016/j.rser.2014.09.042. (2015).
9. Akhtar, N., Geyer, B. & Schrum, C. Impacts of accelerating deployment of offshore windfarms on near-surface climate. *Sci. Rep.* **12**, 18307 (2022).
10. Akhtar, N., Geyer, B., Rockel, B., Sommer, P. & Schrum, C. Accelerating deployment of offshore wind energy alter wind climate and reduce future power generation potentials. *Sci. Rep*. https://doi.org/10.1038/s41598-021-91283-3. (2021).

11. Nygaard, N. G. & Hansen, S. D. Wake effects between two neighbouring wind farms. *J. Phys. Conf. Ser.* **753**, 032020 (2016).
12. Lundquist, J. K., DuVivier, K. K., Kaffine, D. & Tomaszewski, J. M. Costs and consequences of wind turbine wake effects arising fromuncoordinated wind energy development. *Nat. Energy* **4**, 26–34 (2019).
13. Daewel, U., Akhtar, N., Christiansen, N. & Schrum, C. Offshore wind farms are projected to impact primary production and bottom water deoxygenation in the North Sea. *Commun. Earth Environ.* **3**, 292 (2022).
14. Akhtar, N., Geyer, B. & Schrum, C. Larger wind turbines as a solution to reduce environmental impacts. *Sci. Rep.* **14**, 1–12 (2024).
15. Emeis, S. et al. Exploring the Wakes of Large Offshore Wind Farms. In *Journal of Physics: Conference Series*. https://doi.org/10.1088/1742-6596/753/9/092014. (Institute of Physics Publishing, 2016).
16. Platis, A. et al. First in Situ evidence of wakes in the far field behind offshore wind farms. *Sci. Rep*. 8. https://doi.org/10.1038/s41598-018-20389-y. (2018).
17. Rajewski, D. A. et al. Crop Wind Energy Experiment (CWEX): observations of surface-layer, boundary layer, and mesoscale interactions with a wind farm. *Bull. Am. Meteorol. Soc*. 94. https://doi.org/10.1175/BAMS-D-11-00240.1. (2013).
18. Smith, C. M., Barthelmie, R. J. & Pryor, S. C. In situ observations of the influence of a large onshore wind farm on near-surface temperature, turbulence intensity and wind speed profiles. *Environ. Res. Lett.* **8**. https://doi.org/10.1088/1748-9326/8/3/034006. (2013).
19. Armstrong, A. et al. Ground-level climate at a peatland wind farm in scotland is affected by wind turbine operation. *Environ. Res. Lett.* **11**. https://doi.org/10.1088/1748-9326/11/4/044024. (2016).
20. Emeis, S. A simple analytical wind park model considering atmospheric stability. *Wind Energy* **13**, 459–469 (2010).
21. Hasager, C., Rasmussen, L., Peña, A., Jensen, L. & Réthoré, P.-E. Wind farm wake: the horns rev photo case. *Energies* **6**, 696–716 (2013).
22. Foreman, R. J., Cañadillas, B., Neumann, T. & Emeis, S. Measurements of heat and humidity fluxes in the wake of offshore wind turbines. *J. Renew. Sustain. Energy* **9**. https://doi.org/10.1063/1.5003811 (2019).
23. Siedersleben, S. K. et al. Micrometeorological impacts of offshore wind farms as seen in observations and simulations. *Environ. Res. Lett.* **13**. https://doi.org/10.1088/1748-9326/aaea0b (2018).
24. FACT CHECK: there is no direct evidence that offshore windfarms cause heavier rainfall on land. Accessed 29 June 2026. https://www.vrt.be/vrtnws/en/2023/03/15/fact-check-there-is-no-direct-evidence-that-offshore-windfarms/.
25. Fitch, A. C., Olson, J. B. & Lundquist, J. K. Parameterization of wind farms in climate models. *J. Clim.* **26**, 6439–6458 (2013).
26. Seo, H., Sauvage, C., Renkl, C., Lundquist, J. K. & Kirincich, A. Sea surface warming and ocean-to-atmosphere feedback driven by large-scale offshore wind farms under seasonally stratified conditions. *Sci. Adv*. **11**. https://doi.org/10.1126/sciadv.adw7603 (2025).
27. Akhtar, N., Geyer, B., Rockel, B., Sommer, P. S. & Schrum, C. Accelerating deployment of offshore wind energy alter wind climate and reduce future power generation potentials. *Sci. Rep*. **11**. https://doi.org/10.1038/s41598-021-91283-3 (2021).
28. Borgers, R. et al. Mesoscale modelling of north sea wind resources with COSMO-CLM: model evaluation and impact assessment of future wind farm characteristics on cluster-scale wake losses. *Wind Energy Sci.* **9**, 697–719 (2024).
29. Platis, A. et al. Long-range modifications of the wind field by offshore wind parks – results of the project WIPAFF. *Meteorologische Z*. https://doi.org/10.1127/metz/2020/1023 (2020).
30. Pan, Y., Yan, C. & Archer, C. L. Precipitation reduction during Hurricane harvey with simulated offshore wind farms. *Environ. Res. Lett.* **13**. https://doi.org/10.1088/1748-9326/aad245 (2018).
31. Al Fahel, N. & Archer, C. L. Observed onshore precipitation changes after the installation of offshore wind farms. *Bull. Atmos. Sci. Technol.* **1**, 179–203 (2020).
32. Rockel, B., Will, A. & Hense, A. The regional climate model COSMO-CLM (CCLM). *Meteorologische Z.* **17**, 347–348 (2008).
33. Geyer, B., Weisse, R., Bisling, P. & Winterfeldt, J. Climatology of North Sea Wind Energy Derived from a Model Hindcast for 1958-2012. *J. Wind Eng. Ind. Aerodyn.* **147**, 18–29 (2015).
34. Geyer, B. High-resolution atmospheric reconstruction for Europe 1948–2012: CoastDat2. *Earth Syst. Sci. Data* **6**, 147–164 (2014).
35. Akhtar, N. & Chatterjee, F. Wind farm parametrization in COSMO5.0_clm15. https://doi.org/10.35089/WDCC/WindFarmPCOSMO5.0clm15. (2020).
36. Leiding, T. et al. Standardization and Comparative Analysis of the Meteorological FINO Measurement Data (FINO123). Final Project Report, German Weather Service (DWD), Hamburg, Germany. https://www.dwd.de/DE/klimaumwelt/klimaforschung/klimaueberwachung/finowind/finodoku/abschlussbericht_pdf.pdf?__blob=publicationFile&v=3 (2016).
37. Elizalde, A., Akhtar, N., Geyer, B. & Schrum, C. Uncertainty in North Sea offshore wind power: contributions of reanalysis forcing, turbine type, and wake parameterization. *Wind Energy Sci.* **11**, 1077–1095 (2026).
38. Doms, G., Schättler, U. & Baldauf, M. A. Description of the nonhydrostatic regional COSMO Model. http://www.cosmo-model.org. (2011).
39. Charnock, H. Wind stress on a water surface. *Q. J. R. Meteorol. Soc*. https://doi.org/10.1002/qj.49708135027. (1955).
40. Elizalde, A. Wind farm parametrization for COSMO6.0-clm [Computer software]. Zenodo. https://doi.org/10.5281/zenodo.10069391. (2023).
41. Gaertner, E. et al. Definition of the IEA 15-Megawatt Offshore Reference Wind Turbine. Wind Energy. Accessed 29 June 2026. https://docs.nlr.gov/docs/fy20osti/75698.pdf.
42. Jonkman, J., Butterfield, S., Musial, W. & Scott, G. Definition of a 5-MW Reference Wind Turbine for Offshore System Development. National Renewable Energy Laboratory (NREL), Technical Report NREL/TP-500-38060 https://docs.nlr.gov/docs/fy09osti/38060.pdf (2009).
43. 4c offshore. Accessed 29 June 2026. https://map.tgs4c.com/offshorewind/.
44. Siegismund, F. & Schrum, C. Decadal changes in the wind forcing over the North Sea. *Clim. Res.* **18**, 39–45 (2001).
45. Christensen, O. B., Kjellström, E., Dieterich, C., Gröger, M. & Meier, H. E. M. Atmospheric regional climate projections for the Baltic Sea Region until 2100. *Earth Syst. Dyn.* **13**, 133–157 (2022).
46. IPCC Working group-I. In *IPCC Sixth Assessment Report.* Accessed 29 June 2026. https://www.ipcc.ch/working-group/wg1/.

Acknowledgements
The authors gratefully acknowledge the German Climate Computing Center (DKRZ) for providing computational resources and storage capacities. This work used resources of the Deutsches Klimarechenzentrum (DKRZ) granted by its Scientific Steering Committee (WLA) under project ID bg1315. Further, datasets provided by the CLM-Community via the DKRZ data pool were used. We also thank Andreas Will for fruitful discussions and suggestions. We thank the anonymous reviewers for their helpful comments and suggestions, and we also thank Philipp Heinrich and Dmitrii Kovalevski for the valuable discussions regarding the reviewers' proposals.

Author contributions
N.A. led the design and analysis of the atmospheric simulations. A.E. was responsible for implementing the wind farm parameterization within the COSMO6-CLM model. B.G. contributed by providing the necessary forcing data and supporting the analytical process. C.S. initiated and supervised the

project throughout its development. N.A. also drafted the initial version of the manuscript. All authors were actively involved in the collaborative writing, reviewing, and editing of the final manuscript.

Funding
This study is funded by the German Federal Ministry of Research, Technology and Space (BMFTR) as part of the project CoastalFutures (grant number 03F0911E) and contributes to the Helmholtz Research Program "Changing Earth – Sustaining our Future." It also forms a contribution to the 'CliCCS—Climate, Climatic Change, and Society' Excellence Cluster at the University of Hamburg, funded by the DFG under Germany's Excellence Strategy (EXC 2037, project number 390683824). Specifically, it supports the CliCCS subproject 'C3 – Sustainable adaptation scenarios for coastal areas', the Research Mission 'Sustainable Use of Marine Areas', and the Coastal Futures project of the German Marine Research Alliance (DAM). Open Access funding enabled and organized by Projekt DEAL.

Competing interests
The authors declare no competing interests

Additional information
Supplementary information The online version contains supplementary material available at https://doi.org/10.1038/s43247-026-03852-x.

Correspondence and requests for materials should be addressed to Naveed Akhtar.

Peer review information *Communications Earth & Environment* thanks Joshua J. Wimhurst and the other, anonymous, reviewer(s) for their contribution to the peer review of this work. Primary Handling Editors: Min-Hui Lo and Nandita Basu. A peer review file is available.

Reprints and permissions information is available at http://www.nature.com/reprints

Publisher's note Springer Nature remains neutral with regard to jurisdictional claims in published maps and institutional affiliations.

Open Access This article is licensed under a Creative Commons Attribution 4.0 International License, which permits use, sharing, adaptation, distribution and reproduction in any medium or format, as long as you give appropriate credit to the original author(s) and the source, provide a link to the Creative Commons licence, and indicate if changes were made. The images or other third party material in this article are included in the article's Creative Commons licence, unless indicated otherwise in a credit line to the material. If material is not included in the article's Creative Commons licence and your intended use is not permitted by statutory regulation or exceeds the permitted use, you will need to obtain permission directly from the copyright holder. To view a copy of this licence, visit http://creativecommons.org/licenses/by/4.0/.

© The Author(s) 2026